PHYSICAL REVIEW B **91**, 201408(R) (2015)

Frequency pulling and line-shape broadening in graphene Raman spectra by resonant Stokes surface plasmon polaritons

Behnood G. Ghamsari,[1,2,*] Anthony Olivieri,[1,2] Fabio Variola,[3,4] and Pierre Berini[1,2,4,†]

[1]*School of Electrical Engineering and Computer Science, University of Ottawa, 800 King Edward Avenue, Ottawa, Ontario, Canada K1N 6N5*

[2]*Centre for Research in Photonics at the University of Ottawa, 800 King Edward Avenue, Ottawa, Ontario, Canada K1N 6N5*

[3]*Department of Mechanical Engineering, University of Ottawa, 161 Louis Pasteur Street, Ottawa, Ontario, Canada K1N 6N5*

[4]*Department of Physics, University of Ottawa, 150 Louis Pasteur Street, Ottawa, Ontario, Canada K1N 6N5*

(Received 24 February 2015; revised manuscript received 3 March 2015; published 21 May 2015)

This Rapid Communication reports on the modulation of the position and linewidth of the G and $2D$ Raman bands for monolayer graphene through coupling to surface plasmon polaritons (SPPs). It is shown that gold nanoresonators tuned to the graphene Stokes emission frequency, not the laser pump, broaden the G and $2D$ peaks and shift them to lower wave numbers, in addition to enhancing the Raman scattering cross section. The variation of the band displacement and broadening with the SPPs' frequency demonstrates a strongly dispersive phenomenon, ruling out chemical, mechanical, and thermal mechanisms. It is believed that strong graphene-SPP coupling is responsible for the frequency pulling and line-shape broadening.

DOI: 10.1103/PhysRevB.91.201408 PACS number(s): 78.67.Wj, 73.20.Mf, 78.30.−j, 78.66.−w

Raman spectroscopy has been an important tool for studying graphene. It is well known that the precise position and line shape of the D, G, and $2D$ bands, corresponding to about 1350, 1580, and 2700 cm^{-1} wave-number shifts, respectively, can reveal the wide variety of graphene's properties, ranging from the number of layers and degree of disorder to doping level and electron-phonon coupling [1–5]. Interestingly, graphene has also been shown to enhance Raman scattering in adsorbent molecules through a charge transfer mechanism [6]. The chemical origin of this mechanism has been demonstrated by the dependence of the enhancement factor on graphene's Fermi level as well as by comparison to similar phenomena on polar two-dimensional substrates such as BN and MoS_2 where dipole-dipole interactions dominate [7,8]. This phenomenon has attracted much interest for surface-enhanced Raman spectroscopy [9]. In order to obtain increasingly higher Raman enhancement factors towards the achievement of single-molecule sensitivity, other strategies have been explored to complement the *chemical mechanism*. Since surface plasmon polaritons (SPPs) have been proven as an efficient and viable means to enhance optical processes in graphene [10–13], the *electromagnetic mechanism* has been developed for Raman enhancement based on metal nanostructures [14–17]. This mechanism originates from the enhanced local field produced by the SPP resonances of the nanostructures at the pump laser wavelength, which, in turn, results in the enhancement of Raman scattering due to the nonlinear dependence of the induced optical polarization on the incident field. Moreover, it has been recently demonstrated that utilizing nanostructures whose SPP resonances are tuned to the Stokes wavelengths, rather than the pump wavelength, equally efficiently enhance Raman scattering through an alternative mechanism based on increasing the optical density of states at the emission frequency [18]. This mechanism is similar in nature to the Purcell effect where the increased density of states provided by an electromagnetic cavity enhances the rate of spontaneous emission from a quantum emitter [19]. While both electromagnetic Raman enhancement mechanisms rely on SPP resonances of metal nanostructures, they may, however, be experimentally distinguished by the drastically asymmetric enhancement of the G and $2D$ bands that characterizes the latter. Such enhancement asymmetry stems from the significant spectral separation between the G and $2D$ Stokes wavelengths, and from the fact that only one of them (at any given time) can be spectrally aligned to a SPP resonance on a metal nanostructure. For instance, with a pump laser at 633 nm, the Stokes wavelengths associated with the G and $2D$ bands are ∼703 and 763 nm, respectively. The ∼34 THz (60 nm) distance between the two Raman bands allows for selective enhancement provided that the Stokes-tuned SPP resonance is sufficiently narrow. Conversely, a resonance tuned to the pump wavelength will enhance both bands equally.

Aside from the applied significance of the resulting Raman enhancement, selective coupling of SPPs to either of the G and $2D$ bands can reveal interesting insights into the interaction of graphene with SPPs. This Rapid Communication demonstrates the coherent interaction between graphene and SPPs by examining the center and linewidth of the G and $2D$ peaks for monolayer graphene coupled to resonant metal nanostructures. It was observed that the SPPs soften both Raman bands, i.e., reducing the G and $2D$ wave-number shifts. The frequency pulling effect was more pronounced for the G band, resulting in a shift as high as 11 cm^{-1}. The $2D$ band was also shifted in the same direction albeit to a lesser extent. The shift in the Raman bands was accompanied by a broadening of the line shapes for both the G and $2D$ peaks. The dispersive nature of the interaction was investigated by varying the nanostructures' SPP resonance over the intrinsic Stokes frequency. This was achieved by scaling the dimensions of the plasmonic nanoresonators. It was observed that the variations of both the band displacement and broadening versus the SPP resonant wavelength followed Lorentzian line shapes centered near the intrinsic Stokes wavelengths. In fact, the band displacement and broadening maxima coincide with each other as well as with the maximum of the enhancement factor. This result excludes several possible mechanisms that have been recently

*ghamsari@uottawa.ca
†pberini@uottawa.ca

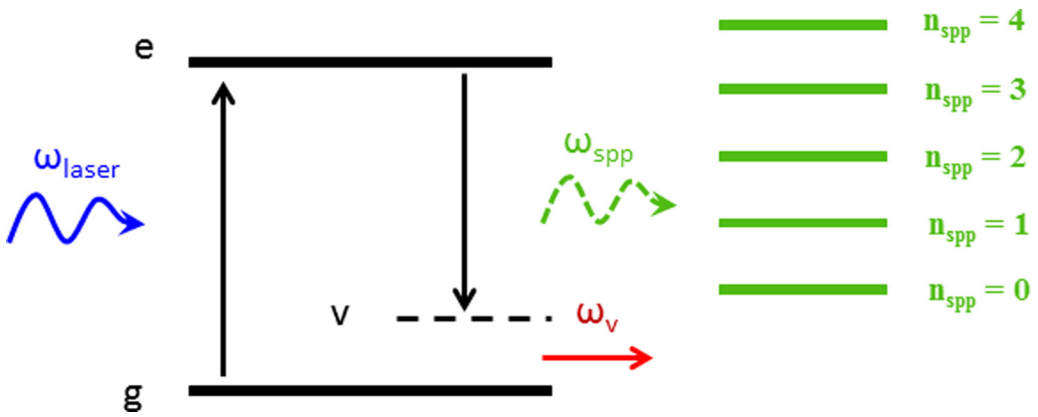

FIG. 1. (Color online) Schematic representation of enhanced Stokes scattering through resonant coupling to a surface plasmon polariton (SSP) nanoresonator at $\omega_{spp} \cong \omega_{Stokes}$. A pump photon at ω_{laser} is absorbed by graphene and a Stokes surface plasmon polariton (SSPP) at ω_{spp} is created in the plasmonic resonator. The resonator, in turn, radiates SSPPs as photons into the free space through its induced electric dipole moment.

reported to explain Raman band displacement in graphene due to chemical, thermal, and strain effects [20–22]. These mechanisms are ruled out here because the band displacement and broadening effects only appear for nanostructures with SPP resonant frequencies close to the Stokes wavelengths. A minor change in the dimensions of the nanostructures (to slightly larger or smaller) disrupts their spectral alignment with the intrinsic Stokes wavelength and restores the intrinsic line shapes. Thermal mechanisms could, in fact, be responsible for band displacement and broadening in Raman enhancement schemes where the plasmonic nanostructures are resonant to the pump laser wavelength. However, heating effects are not expected to play a significant role in our experiment since none of the nanostructures resonate with the pump laser. Furthermore, the electromagnetic power in the Stokes wavelengths is of the order of 5 nW, much weaker than that required to raise the temperature of graphene.

Therefore, we believe that strong graphene-SPP coupling underlies the band displacement and broadening. As illustrated schematically in Fig. 1, the presence of plasmonic nanoresonators modifies the graphene Raman process by scattering the incident photons into Stokes surface plasmon polaritons (SSPPs).

In our measurements, we have used arrays of rectangular gold nanoresonators on monolayer graphene, grown by chemical vapor deposition over a 285-nm-thick layer of thermally grown silicon dioxide on a silicon substrate. The nanoresonators are 22 nm thick, 40 or 55 nm wide, and of a length that varies from 58 to 118 nm. Figure 2(a) sketches the unit cell containing a single nanoresonator. For each combination of length and width, the nanoresonators were arranged in a 40×40 square array spanning a $20 \times 20\,\mu m^2$ area. The separation between adjacent cells was sufficiently large to ensure that nanoresonators were isolated from their neighbors and resonated independently. The nanoresonators operated as half-wavelength monopole antennas supporting SPPs that resonate in a dipolar mode [23].

The nanostructures were fabricated by electron-beam lithography using a bilayer PMMA resist followed by metal evaporation and lift-off. Figure 2(b) displays a SEM image of a typical nanoresonator array. Figure 2(c) shows the nanostructures' resonance wavelength as a function of their length and width based on three-dimensional full-wave finite-element method electromagnetic simulation. The measurements were carried out using a confocal Raman microscope (WITec Alpha 300R) and a He-Ne laser. The laser power impinging on the samples from free space was ∼5 mW. The beam was focused onto an approximately 1-μm-diameter spot and was raster scanned over the samples in 100-nm steps to obtain a two-dimensional image of the Raman spectrum. More details about the fabrication and measurement steps as well as the linear response of similar devices, including reflection and transmission characteristics and their geometrical scaling rules, can be found elsewhere [18,23].

Figure 3(a) shows the measured Raman enhancement factor as a function of the nanostructures' resonance wavelength. The enhancement factor associated with an individual nanoresonator was calculated by taking a bare graphene area without any plasmonic nanostructures as the reference according to Ref. [18]. The enhancement factors are evidently maximized where the nanostructures' resonance wavelength coincides with the corresponding G or $2D$ Stokes wavelength. This confirms that the Raman enhancement mechanism, herein, is dominated by the resonant Stokes emission as previously discussed [18], and the SPP resonances are adequately narrow to resolve the spectral distance between the G and $2D$ bands.

Figure 4 provides the measured Raman signals in the G and $2D$ bands as a function of the nanostructures' resonant wavelength. The line shapes are not significantly altered by the metal nanostructures when the SPP resonances lie far from the intrinsic Stokes wavelength. As the Stokes wavelength is approached, the peaks broaden and displace to lower wave numbers. Figures 5 and 6 display the displacement of the peak center and its full width at half maximum (FWHM) for both Raman bands, for two sets of nanoresonators both consisting of devices with a length in the range from 58 to 118 nm but differing in width, viz., 40 and 55 nm wide. The variations of the band center and FWHM with the SPP resonant wavelength can be well fitted with Lorentzian functions centered near the intrinsic Stokes wavelengths. As the spectral alignment with the intrinsic Stokes wavelengths is lost (in slightly longer or shorter nanoresonators), the displacement and broadening

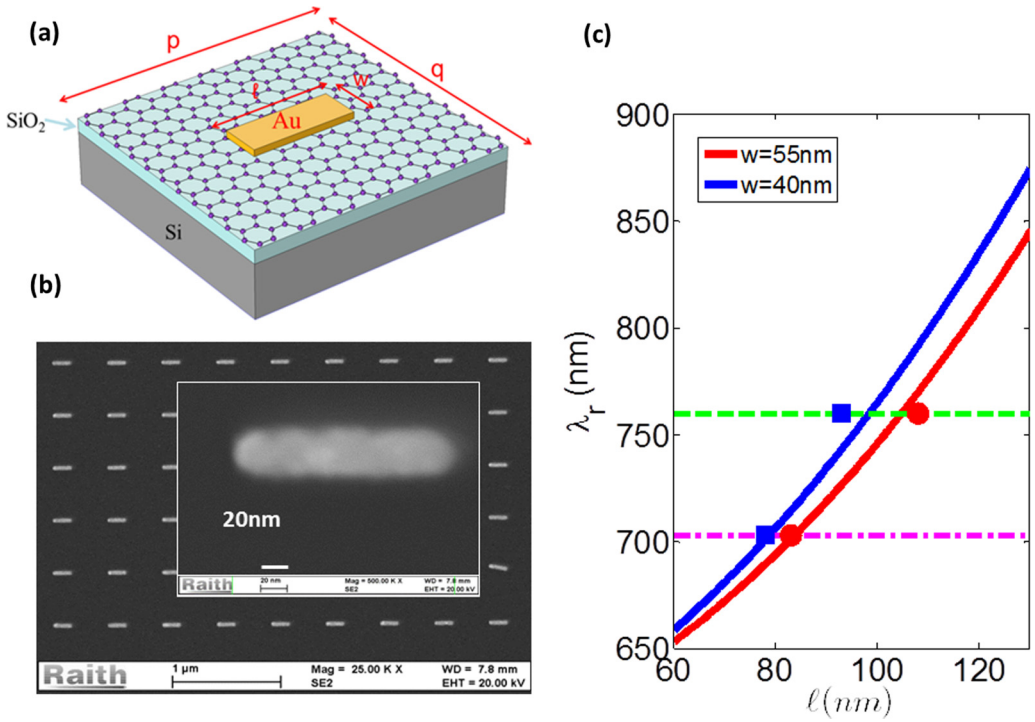

FIG. 2. (Color online) (a) Schematic representation of a half-wavelength SPP nanoresonator. (b) SEM image of a nanoresonator array. The inset shows an individual nanoresonator of the array. (c) Resonant wavelength vs length for 22-nm-thick gold nanoresonators of width 40 nm (blue) and 55 nm (red) as obtained from three-dimensional full-wave electromagnetic simulation. Dashed horizontal lines show the G (magenta) and $2D$ (green) Stokes wavelengths for a pump laser at 633 nm. The circles and squares mark the resonator lengths associated with the maximum measured enhancement factors.

rapidly diminish and the spectra converge to their unperturbed line shapes.

There are several reported thermal, chemical, and mechanical mechanisms that could potentially lead to related effects in the graphene Raman spectrum [4,20–22]. Here, we examine their possible contribution to our measurements. Heating the graphene sample by means of SPP dissipation and, thereby, disturbing the phonon modes can be readily ruled out due to several reasons. First, none of the nanostructures resonantly interact with the pump field. This is evident from Fig. 2(c) showing that none of the SPP resonances lies close to the pump wavelength. Figure 3 further corroborates the lack of resonant interaction with the pump laser beam by exhibiting no experimental enhancement in the Raman signal for any nanoresonator other than those very close to the Stokes wavelengths. The measured enhancement factor is, indeed, the lowest for the SPP resonances closest to the pump wavelength, i.e., farthest away from the Stokes wavelengths. Heating by means of Ohmic dissipation at the Stokes wavelengths can also be ruled out because of the small cross section of the scattering and, thus, the small fraction of the incident power scattered to the Stokes wavelength (estimated well below 5 nW). This argument is further reinforced by observing that between the two sets of the nanoresonators of different width, the one inducing the larger broadening leads to a smaller band displacement. This result clearly excludes bolometric mechanisms. Noteworthy, nonresonant heating due to a laser beam being focused into a small spot may still, however, affect the measurements, but it would equally influence the measured Raman spectra regardless of nanoresonator dimensions. As discussed below, this mechanism is expected to only have a marginal role in the observed displacement and broadening.

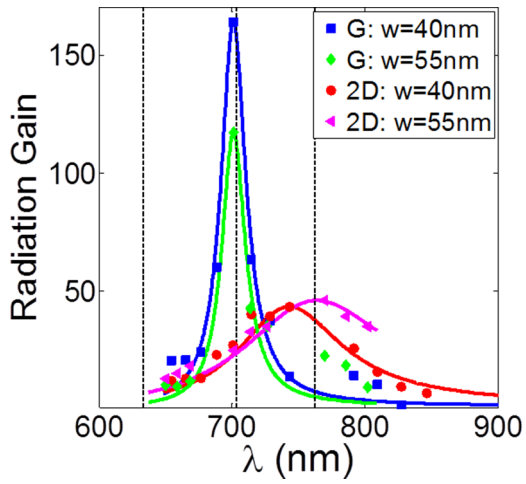

FIG. 3. (Color online) Effective enhancement of Raman scattering cross section per nanoresonators as a function of their resonant wavelength. The dashed vertical lines mark the laser line, G peak, and $2D$ peak wavelengths, respectively, from left to right.

It is known that the presence of metal nanoparticles can affect the graphene Raman spectrum through chemical doping and/or mechanical strain [20–22]. By examining the residual displacement and broadening for the nanostructures with the largest frequency detuning in Figs. 5 and 6, an upper bound of $\sim$1.5 and 3 cm^{-1} can be found for the aggregate contributions

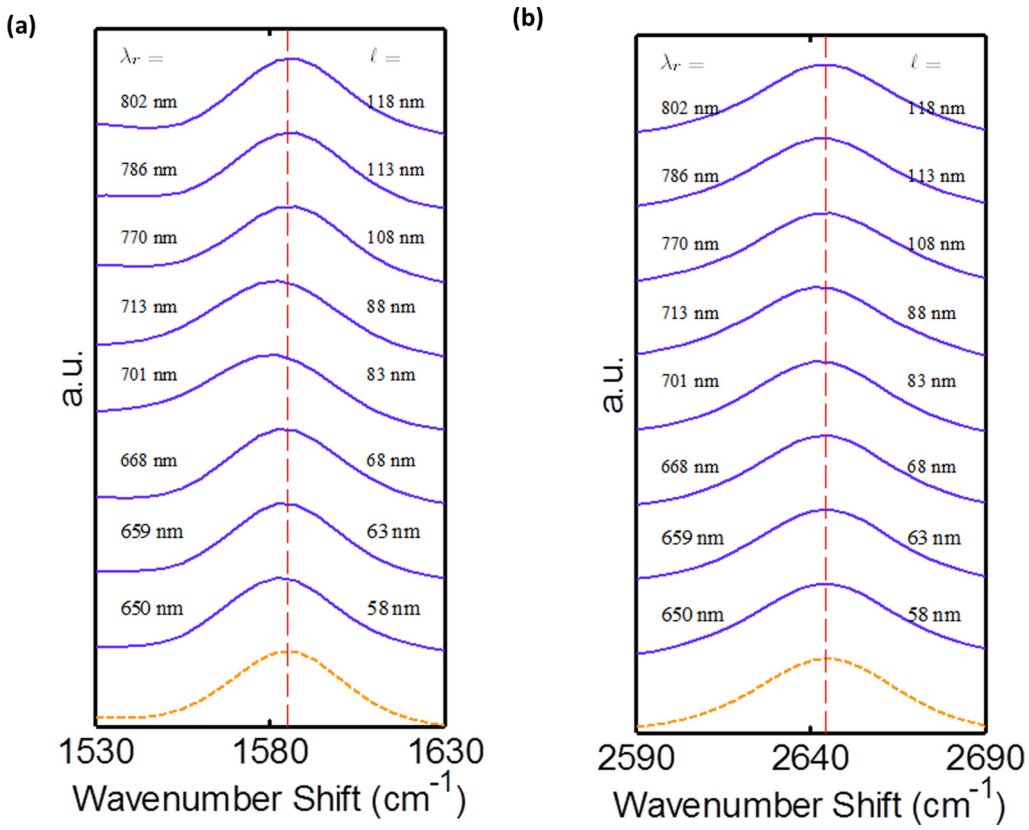

FIG. 4. (Color online) Evolution of the (a) G and (b) $2D$ peaks with the SPP resonant wavelength associated with 55-nm-wide nanostructures. The spectra were normalized to have equal heights. The resonant wavelengths (on the left) are related to the nanoresonators' physical lengths (on the right) via the computations of Fig. 2(c). The dashed-line curve at the bottom corresponds to a control graphene region with no nanostructures in the vicinity. The vertical dashed line represents the control region peak position (intrinsic Stokes wavelengths in graphene).

of chemically, mechanically, and thermally induced perturbations to the band center and linewidth, respectively. Since a displacement and broadening as high as 11 and 30 cm^{-1}, respectively, were detected for the G band, we can conclude that the observed effects are predominantly due to interactions with SPPs. The Lorentzian dispersion of the displacement and broadening as well as their close correlation with the associated Raman enhancement factor further confirm the resonant coupling between SPPs and graphene at the Stokes frequency.

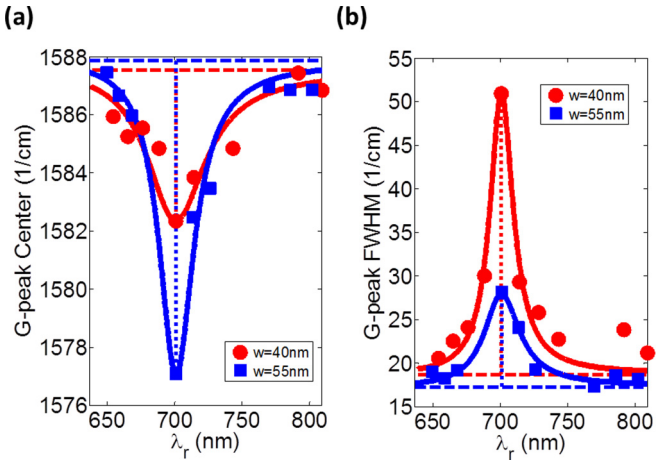

FIG. 5. (Color online) Variation of the G-peak (a) center and (b) full width at half maximum (FWHM) as a function of the SPP resonant wavelength supported by the nanoresonators. Solid lines are Lorentzian curves used to fit the experimental data.

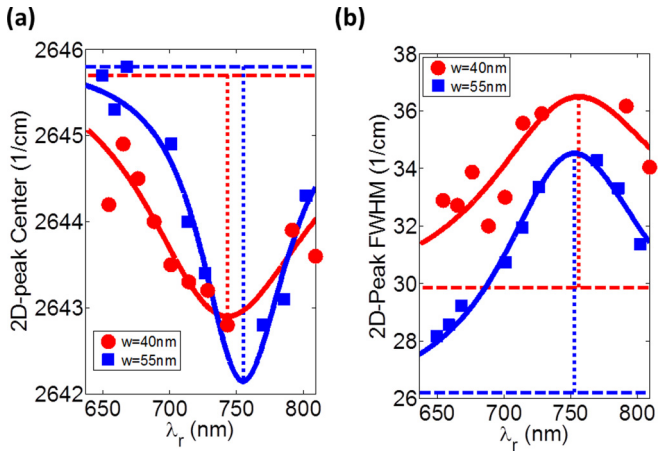

FIG. 6. (Color online) Variation of the $2D$-peak (a) center and (b) full width at half maximum (FWHM) as a function of the SPP resonant wavelength supported by the nanoresonators. Solid lines are Lorentzian curves used to fit the experimental data.

Upon introducing the SPP nanoresonators, the Stokes emission is no longer generated by radiation of redshifted photons into free space, but instead by the creation of Stokes surface plasmon polaritons (SSPPs) in the plasmonic mode of the nanoresonators. The induced dipole moment in the nanoresonators, in turn, gives rise to radiation of photons, which are detected by the Raman apparatus in the far field. This process is schematically illustrated in Fig. 1. The enhanced Raman cross section, in fact, is the direct consequence of the higher optical density of states provided by the nanoresonators (cavity) compared to free space. The increased linewidth of the measured photons is thus caused by damping of SPPs in the nanoresonators. The steady-state population of SPPs in the plasmonic nanoresonator is determined by the interplay of the rate of SSPPs emission from graphene into the plasmonic nanostructures, the damping rate of the SPPs, and the dipole radiation loss. The steady-state population also characterizes the graphene-SPP coupling strength. Therefore, a higher damping rate, which results in a lower steady-state SPP accumulation, corresponds to a weaker coupling between SPPs and graphene. This result explains the lower band displacement measured from the nanoresonator set exhibiting the greater broadening, as shown in Figs. 5 and 6.

In summary, we have shown that plasmonic nanoresonators tuned to the Stokes wavelengths broaden the G and $2D$ Raman bands in graphene and displace them to lower wave numbers. The variation of the displacement and broadening with the resonance frequency of the nanostructures follows Lorentzian functions, ultimately indicating a strongly dispersive interaction between SPPs and graphene. The coincidence of the enhancement, frequency pulling, and linewidth broadening were carefully examined to evaluate the possible contribution of thermal, chemical, and mechanical mechanisms. As all of these mechanisms were ruled out as the main contributing factors, the observed phenomena are attributed to the scattering of the incident pump photons into Stokes surface plasmon polaritons assisted by graphene optical phonons.

The work of B.G.G., F.V., and P.B. is, in part, supported by the Natural Sciences and Engineering Research Council of Canada. F.V. acknowledges financial support from the Canada Foundation for Innovation (CFI) and the Ontario Ministry of Research and Innovation (MRI) through the Leaders of Opportunity (LOF) fund.

[1] A. C. Ferrari, J. C. Meyer, V. Scardaci, C. Casiraghi, M. Lazzeri, F. Mauri, S. Piscanec, D. Jiang, K. S. Novoselov, S. Roth, and A. K. Geim, Phys. Rev. Lett. **97**, 187401 (2006).

[2] J. Yan, Y. Zhang, P. Kim, and A. Pinczuk, Phys. Rev. Lett. **98**, 166802 (2007).

[3] A. Das, S. Pisana, B. Chakraborty, S. Piscanec, S. K. Saha, U. V. Waghmare, K. S. Novoselov, H. R. Krishnamurthy, A. K. Geim, A. C. Ferrari, and A. K. Sood, Nat. Nanotechnol. **3**, 210 (2008).

[4] M. Hulman, M. Haluška, G. Scalia, D. Obergfell, and S. Roth, Nano Lett. **8**, 3594 (2008).

[5] M. S. Dresselhaus, A. Jorio, M. Hofmann, G. Dresselhaus, and R. Saito, Nano Lett. **10**, 751 (2010).

[6] X. Ling, L. Xie, Y. Fang, H. Xu, H. Zhang, J. Kong, M. S. Dresselhaus, J. Zhang, and Z. Liu, Nano Lett. **10**, 553 (2010).

[7] Q. Hao, S. M. Morton, B. Wang, Y. Zhao, L. Jensen, and T. J. Huang, Appl. Phys. Lett. **102**, 011102 (2013).

[8] X. Ling, W. Fang, Y.-H. Lee, P. T. Araujo, X. Zhang, J. F. Rodriguez-Nieva, Y. Lin, J. Zhang, J. Kong, and M. S. Dresselhaus, Nano Lett. **14**, 3033 (2014).

[9] W. Xu, N. Mao, and J. Zhang, Small **9**, 1206 (2010).

[10] F. Bonaccorso, Z. Sun, T. Hasan, and A. C. Ferrari, Nat. Photonics **4**, 611 (2010).

[11] A. N. Grigorenko, M. Polini, and K. S. Novoselov, Nat. Photonocs **6**, 749 (2012).

[12] X. Gan, R.-J. Shiue, Y. Gao, K. F. Mak, X. Yao, L. Li, A. Szep, D. Walker, Jr., J. Hone, T. F. Heinz, and D. Englund, Nano Lett. **13**, 691 (2013).

[13] Z. Fang, Z. Liu, Y. Wang, P. M. Ajayan, P. Nordlander, and N. J. Halas, Nano Lett. **12**, 3808 (2012).

[14] V. Kravets, F. Schedin, R. Jalil, L. Britnell, K. S. Novoselov, and A. N. Grigorenko, J. Phys. Chem. C **116**, 3882 (2012).

[15] A. Urich, A. Pospischil, M. M. Furchi, D. Dietze, K. Unterrainer, and T. Muellerb, Appl. Phys. Lett. **101**, 153113 (2012).

[16] C.-E. Cheng, C.-Y. Lin, H.-Y. Chang, C.-H. Huang, H.-Y. Lin, C.-H. Chen, C.-C. Hsu, C.-S. Chang, and F. S.-S. Chien, Opt. Express **21**, 6547 (2013).

[17] S. Heeg, R. Fernandez-Garcia, A. Oikonomou, F. Schedin, R. Narula, S. A. Maier, A. Vijayaraghavan, and S. Reich, Nano Lett. **13**, 301 (2013).

[18] B. G. Ghamsari, A. Olivieri, F. Variola, and P. Berini, Nanophotonics **3**, 363 (2014).

[19] E. M. Purcell, Phys. Rev. **69**, 681 (1946).

[20] Z. H. Ni, T. Yu, Y. H. Lu, Y. Y. Wang, Y. P. Feng, and Z. X. Shen, ACS Nano **2**, 2301 (2008).

[21] S. G. Zhang, X. W. Zhang, X. Liu, Z. G. Yin, H. L. Wang, H. L. Gao, and Y. J. Zhao, Appl. Phys. Lett. **104**, 121109 (2014).

[22] C. Qiu, H. Zhou, B. Cao, L. Sun, and T. Yu, Carbon **59**, 487 (2013).

[23] S. S. Mousavi, P. Berini, and D. McNamara, Opt. Express **20**, 18044 (2012).